Quantum Electronic Structure

Assessment of Density Functional Theory in Predicting Interaction Energies Between Water and Polycyclic Aromatic Hydrocarbons: From Water on Benzene to Water on Graphene

Adeayo O. Ajala, Vamsee K Voora, Narbe Mardirossian, Filipp Furche, and Francesco Paesani

Just Accepted

Assessment of Density Functional Theory in Predicting Interaction Energies Between Water and Polycyclic Aromatic Hydrocarbons: From Water on Benzene to Water on Graphene

Adeayo O. Ajala,*,† Vamsee Voora,‡ Narbe Mardirossian,¶ Filipp Furche,‡ and Francesco Paesani*,†,§,∥

†Department of Chemistry and Biochemistry, University of California San Diego, La Jolla, California 92093, United States

‡Department of Chemistry, University of California Irvine, Irvine, California 92697, United States

¶Division of Chemistry and Chemical Engineering, California Institute of Technology, 1200 E. California Boulevard, Pasadena, California 91125, United States

§Materials Science and Engineering, University of California San Diego, La Jolla, California 92093, United States

∥San Diego Supercomputer Center, University of California San Diego, La Jolla, California 92093, United States

E-mail: aajala@ucsd.edu; fpaesani@ucsd.edu

Abstract

The interactions of water with polycyclic aromatic hydrocarbons, from benzene to graphene, are investigated using various exchange-correlation functionals selected across the hierarchy of density functional theory (DFT) approximations. The accuracy of the different functionals is assessed through comparisons with random phase approximation (RPA) and coupled-cluster with single, double, and perturbative triple excitations [CCSD(T)] calculations. Diffusion Monte Carlo (DMC) data reported in the literature are also used for comparison. Relatively large variations are found in interaction energies predicted by different DFT models, with GGA functionals underestimating the interaction strength for configurations with the water oxygen pointing toward the aromatic molecules. The meta-GGA B97M-rV and range-separated hybrid, meta-GGA ωB97M-V functionals provide nearly quantitative agreement with CCSD(T) values for the water–benzene, water–coronene, and water–circumcoronene dimers, while RPA and DMC predict interaction energies that differ by up to $\sim$1 kcal/mol and $\sim$0.4 kcal/mol from the corresponding CCSD(T) values, respectively. Similar trends among GGA, meta-GGA, and hybrid functionals are observed for larger polycyclic aromatic hydrocarbons. By performing absolutely localized molecular orbital energy decomposition analyses (ALMO-EDA), it is found that, independently of the number of carbon atoms and exchange-correlation functional, the dominant contributions to the interaction energies between water and polycyclic aromatic hydrocarbon molecules are the electrostatic and dispersion terms while polarization and charge transfer effects are negligibly small. Calculations carried out with GGA and meta-GGA functionals indicate that, as the number of carbon atoms increases, the interaction energies slowly converge to the corresponding values obtained for an infinite graphene sheet.

1 INTRODUCTION

Motivated by potential technological applications, including water desalination, electricity generation, and biochemical sensing, there has recently been significant effort in investigating the properties of water interacting with graphene.[1–18] From a computational modeling perspective, realistic simulations of water at the interface with graphene sheets require an accurate representation of the underlying molecular interactions, at both short and long ranges. Several molecular dynamics (MD) studies, employing either force fields or *ab initio* methods, have been reported to characterize the behavior of water adsorbed on graphene. For example, MD simulations were carried out to investigate the dependence of the contact angle on the strength of carbon–water interactions[19] as well as to determine the importance of polarization effects in the representation of water–graphene interactions.[20] Other studies focused on characterizing the hydrophobic effect on electrically doped graphene layers.[21] MD simulations with the TIP4P water model[22] were used in Ref. 23 to examine the desalination performance of graphene, while water and ion transport through graphene pores was investigated in Refs. 24 and 25. Besides water, the interaction of other polar substances, such as nucleobases, has been investigated in a systematic fashion on graphite-like surfaces.[26]

Most *ab initio* studies of water interacting with graphene rely on density functional theory (DFT). However, it is known that standard exchange-correlation (XC) functionals lack the ability to capture long-range dispersion interactions and thus often underestimate the strength of molecular interactions.[27–30] More reliable results can be obtained by combining standard XC functionals with semi-classical dispersion corrections,[31–34] or by constructing nonlocal XC functionals.[35,36] In this context, it was shown that the performance of different DFT models in describing water–graphene interactions depends not only on the specific XC functional used in the calculations but also on how dispersion forces are accounted for.[37] In particular, it was found that the application of van der Waals DFT models to investigate the interaction of a single water molecule with a graphene sheet gives results that are in good agreement with those obtained with high-level electronic structure methods.[18,37,38]

On the other hand, some discrepancies exist among interaction energies reported in the literature from calculations with high-level electronic structure methods.[15,16,37–39] For instance, in Ref. 37 the binding energy of water on graphene was determined to be 1.61 ± 0.23 kcal/mol and 1.78 kcal/mol from diffusion Monte Carlo (DMC) and random phase approximation (RPA) calculations, respectively. A more recent study[38] from the same group places the DMC and RPA values at 2.28 ± 0.14 and 1.89 ± 0.02 kcal/mol, respectively. The relatively large difference between the DMC estimates was attributed to larger statistical errors (smaller precision) and remaining finite-size effects that affected the older DMC calculations.[38]

By relying on the method of increments[40] and using a 3×3 supercell, coupled-cluster (CC) with single, double, and perturbative triple excitations (CCSD(T)) calculations carried out with a combination of cc-pVDZ and aug-cc-pVTZ basis sets predicted the binding energy of water on graphene to be 2.84 kcal/mol. This value is in line with water–graphene binding energy of 2.7 kcal/mol obtained in Refs. 15 and 16 using density fitting DFT symmetry-adapted perturbation theory and DFT/CC approaches, respectively. Recent p-CCSD(T) calculations, carried out with a larger unit cell (4×4), predicted the binding energy of water on graphene to be ~ 2.0 kcal/mol.[38]

While CCSD(T) interaction energies obtained in the complete basis set limit are considered highly accurate for large-gap molecular compounds and insulators,[41] CCSD(T) calculations are computationally expensive, which precludes their application to large systems and in MD simulations of condensed phase systems. The RPA method[42] based on the adiabatic-connection fluctuation-dissipation theorem (ACFDT)[43] correctly captures many-body dispersion interactions for extended systems and molecules, including metals and insulators.[44–49] The direct or bare RPA is non-perturbative and equivalent to direct ring coupled-cluster doubles,[50] but its computational cost is orders of magnitude below than that of CCSD(T) when used in conjunction with imaginary frequency integration and resolution-of-the-identity methods.[51] Thus, RPA is increasingly used as a cost-efficient first-principles method for

modeling noncovalent interactions in molecules and materials.[52–58] Nevertheless, RPA underestimates dispersion energies[47] as a result of lacking higher excitations and density-driven error[59] inherited from the semilocal Kohn-Sham reference. The latter can be ameliorated by variational selfconsistent RPA[60] or perturbative singles corrections.[61–63] Although some MD simulations at the MP2 and RPA level of theory have been reported,[52,53,64,65] DFT effectively remains the *ab initio* approach of choice for MD simulations of aqueous solutions in periodic boundary conditions.

In this study, we investigate the performance of various generalized gradient approximation (GGA), meta-GGA, hybrid, and range separated hybrid, meta-GGA XC functionals in predicting interaction energies between a single water molecule and a series of polycyclic aromatic hydrocarbons (PAHs), from benzene to graphene. The accuracy of the different XC functionals is established through systematic comparisons with corresponding RPA and CCSD(T) calculations. Available DMC values reported in the literature[38] are also included in the comparisons. Besides enabling a systematic assessment of the performance of different DFT approximations, this study also provides fundamental insights into the nature of the interactions between water and PAHs through the application of the absolutely localized molecular orbital energy decomposition analysis (ALMO-EDA) method.[66,67] The analysis reported in this study could thus serve as a guidance for the development of *ab initio*-based force fields for MD simulations aimed at determining the structure and dynamics of water at graphene interfaces.

2 COMPUTATIONAL DETAILS

2.1 Molecular systems

We consider a graphene sheet with C-C bonds and C-C-C angles set to the experimental values of 1.42 Å and 120°, respectively.[68] In order to investigate the dependence of the the interaction energies as a function of the number of carbon atoms, a series of PAH

molecules are extracted from the graphene sheet and the dangling bonds saturated with hydrogen atoms, fixing the C-H bonds and C-C-H angles to the values of 1.089 Å and 120° as defined in Ref. 69. The resulting PAHs include: C_6H_6 (benzene), $C_{24}H_{12}$ (coronene), $C_{54}H_{18}$ (circumcoronene), $C_{96}H_{24}$ (dicircumcoronene), $C_{150}H_{30}$, and $C_{216}H_{36}$. As shown in Fig. 1, three orientations of the water molecule with respect to the plane of each PAH molecule are considered, which are defined as: 0-leg configurations, with the water oxygen pointing towards the central aromatic ring of the PAH molecule and the bisector of the H-O-H angle perpendicular to the plane of the PAH molecule, 1-leg configurations, with one OH bond of the water molecule perpendicular to the plane of the PAH molecule and pointing to one of the carbon atoms of the central aromatic ring, and 2-leg configurations, corresponding to inverted 0-leg configurations, with the two hydrogen atoms pointing towards the central aromatic ring of the PAH molecule. In all calculations, the O-H bonds and H-O-H angle of the water molecule were kept fixed at the gas-phase experimental values of 0.957 Å and 104.5°, respectively. Cartesian coordinates of all water–PAH dimers analyzed in this study are reported in the Supporting Information.
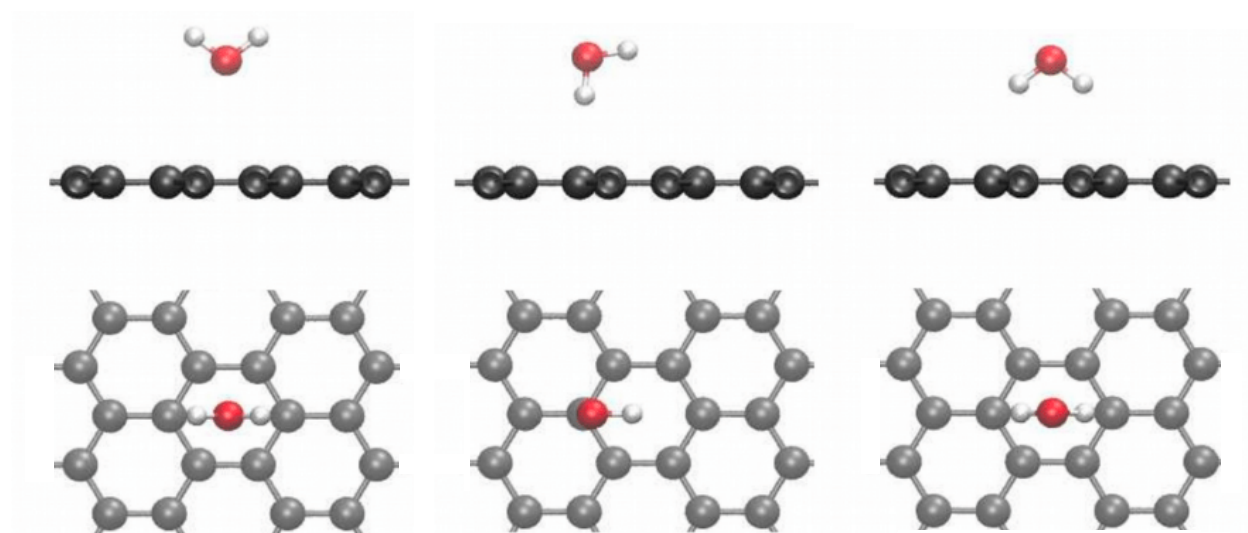
Figure 1: Water orientations considered in this study: 0-leg (left), 1-leg (middle), and 2-leg (right) configurations.

2.2   Density functional theory calculations

We analyze the performance of various XC functionals belonging to the GGA, meta-GGA, hybrid, and range-separated, meta-GGA families. The GGA functionals include: BLYP, which combines Becke exchange functional (B88)[70] with the semilocal Lee-Yang-Parr correlation functional (LYP),[71] the Perdew-Burke-Ernzerhof (PBE) exchange-correlation functional[72] as well as its revised version (revPBE),[73] and the revised Vydrov and van Voorhis functional (rVV10).[74] As representative meta-GGA functionals, we consider the strongly constrained and appropriately normed SCAN functional[75] and the semi-emiprical meta-GGA B97M-V functional, which was recently paired with the rVV10 nonlocal correlation functional.[76] Within the family of hybrid exchange-correlation functionals, we consider B3LYP,[77] PBE0[78] and revPBE0,[79] which are the hybrid analogues of PBE and revPBE, respectively. As a representative of range-separated hybrid, meta-GGA functionals, we consider ωB97M-V.[80] For comparison, calculations of interaction energies between water and the smallest PAH molecules considered in this study are also carried out with the following double hybrid functionals: ωB97X-2(LP) and ωB97X-2(TQZ),[81] and the results are reported in the Supporting Information. To approximate long-range electron correlations associated with dispersion interactions,[82,83] we adopt the D3(0) semiempirical scheme.[32] The corresponding XC functionals with dispersion corrections are indicated as BLYP-D3, PBE-D3, revPBE-D3, SCAN-D3, B3LYP-D3, PBE0-D3, and revPBE0-D3. Calculations with the BJ-damping scheme[84] are also carried out for selected XC functionals and the results are reported in Tables S18 and S19 of the Supporting Information. Comparisons between results obtained with the original D3(0) and BJ damping schemes show that the differences are relatively small, being within $\sim$0.2 kcal/mol for both 0- and 1-leg configurations, independently of the XC functional, and as large as 0.6 kcal/mol in BLYP-D3 and revPBE0-D3 calculations for 2-leg configurations. In the case of SCAN, we also consider the SCAN+rVV10 variant, which is derived by pairing SCAN with the nonlocal correlation part of rVV10.[85]

In the analyses presented in Section 3, the interaction energies, E_{int}, between water and

PAHs are calculated as

$$E_{int} = E_{\text{H}_2\text{O}-\text{PAH}} - E_{\text{H}_2\text{O}}^{(\text{H}_2\text{O}-\text{PAH})} - E_{\text{PAH}}^{(\text{H}_2\text{O}-\text{PAH})} \tag{1}$$

where $E_{\text{H}_2\text{O}-\text{PAH}}$ is the total energy of the H$_2$O–PAH dimer, and $E_{\text{H}_2\text{O}}^{(\text{H}_2\text{O}-\text{PAH})}$ and $E_{\text{PAH}}^{(\text{H}_2\text{O}-\text{PAH})}$ are the energies of the isolated fragments at the same geometries as in the H$_2$O–PAH dimer. All energies are corrected for the basis set superposition error (BSSE) according to the counterpoise scheme of Boys and Bernardi,[86] with the superscripts (H$_2$O–PAH) in Eq. 1 thus indicating that the monomer energies are computed in the dimer basis set. All DFT calculations for the PAH molecules are carried out within the Kohn-Sham formalism as implemented in Q-Chem, version 5.0.[87] We employ the def2-QZVPPD[88] basis set for O and H in water and the surrounding C atoms in the central six-membered ring of the PAH, and the 6-31+G[89,90] basis set for the remaining atoms in the system. As shown in Tables S15–S17 of the Supporting Information, this basis set combination guarantees computational efficiency without compromising accuracy in predicting interaction energies. The DFT calculations of the water–graphene interaction energies are carried out using the QUICKSTEP algorithm[91] as implemented in the CP2K software.[92] For these calculations, we employ augmented quadruple-zeta valence basis sets with three polarization functions (aug-QZV3P) for both water and graphene, while the core electrons are described by the Goedecker-Teter-Hutter pseudopotentials.[93] The calculations are carried out for a 5×5 supercell with dimensions of 12.325 Å×12.325 Å in the $x-y$ plane, and a vacuum region of 25.0 Å in the z-direction.

2.3 Random phase approximation calculations

Direct or bare RPA calculations are carried out for water–C$_6$H$_6$, water–C$_{24}$H$_{12}$, and water–C$_{54}$H$_{18}$ using TURBOMOLE v7.3.[94] The energy calculations use self-consistent PBE[72] orbitals which are computed using m5 grids[95] and an energy-convergence criterion of 10^{-7} a.u.

Explorative selfconsistent spRPA calculations[60] suggested that residual density-driven errors are small. All interaction energies are counterpoise-corrected for BSSE as discussed above, and all core-orbitals were frozen in RPA correlation energy calculations.

Polarized segmented-contracted quadruple-ζ valence (def2-QZVP[96]) basis sets were used throughout for the RPA calculations reported here. def2-QZVP balances accuracy and efficiency for RPA calculations of interaction energies,[97] which is important for applications to larger systems. The basis set incompleteness error of def2-QZVP was assessed for the minimum energy 2-leg wate-benzene and water-coronene complexes, where the use of def2-QZVP leads to a basis set incompleteness error of 0.2 kcal/mol. The complete basis-set limit was estimated using aug-cc-pV(T-Q)Z basis-set extrapolation (see Eq. 2). We note that similar RPA calculations have recently been carried out, although for the H_2O–$C_{24}H_{12}$ and H_2O–$C_{24}H_{12}$ dimers only.[38] Comparisons between the present RPA results and those of Ref. 38 are shown in Section S6 of the Supporting Information.

2.4   Coupled cluster calculations

All CC calculations presented in this study are based on restricted Hartree–Fock reference functions. Interaction energies are calculated for selected H_2O–C_6H_6, H_2O–$C_{24}H_{12}$, and H_2O–$C_{54}H_{18}$ configurations using the linear scaling domain-based pair natural orbital CCSD(T) method, hereafter referred to as L-CCSD(T),[98] as implemented in the ORCA package.[99] Dunning basis sets of cc-pVXZ (where X = D,T,Q,5) quality[100,101] are used in the correlation treatment, while the chemical core is frozen. As a result of linear-dependency problems mentioned in Section 2.3, the cc-pVXZ (X = D,T,Q,5) basis sets are used for H_2O–C_6H_6, the cc-pVXZ (X = D,T,Q) basis sets for H_2O–$C_{24}H_{12}$, and the cc-pVXZ (X = D,T) basis sets for H_2O–$C_{54}H_{18}$. All interaction energies are corrected for the BSSE using Eq. 1. Following Refs. 102 and 103, the complete basis set (CBS) limit of the L-CCSD(T)

interaction energies is achieved by applying the following two-point extrapolation formula:

$$E_0^{(\text{CBS})} = \frac{n^3 E_0^{[\text{cc}n\text{Z}]} - (n-1)^3 E_0^{[\text{cc}(n-1)\text{Z}]}}{n^3 - (n-1)^3}, \tag{2}$$

where n and $(n-1)$ are the cardinal numbers of the cc$n$Z and cc$(n-1)$Z basis sets, respectively. For H_2O–C_6H_6, we extrapolate the results obtained with the largest basis sets by setting $n = 5$ in Eq. 2. Due to the relatively smaller size of the basis sets used for H_2O–$C_{24}H_{12}$, errors that may originate from basis set incompleteness are also taken into account in the (TZ,QZ) extrapolation. These errors are estimated from the difference between (TZ,QZ) and (QZ,5Z) extrapolations carried out for H_2O–C_6H_6. Following Refs. 104 and 105, the ground-state electronic energies of H_2O–$C_{54}H_{18}$ dimer are calculated as

$$E_0 = E_0^{(\text{RHF/QZ})} + \Delta E_0^{(\text{CBS}/(\text{TZ,DZ}))}, \tag{3}$$

where the first term on the right-hand side designates the RHF reference energy obtained using the cc-pVQZ basis set. Due to the fast convergence of the Hartree–Fock energies with respect to the basis set, we can treat the RHF/QZ energies as equivalent to the CBS value. The second term on the right-hand side of Eq. 3 is the CBS limit of the correlation energy and the triples correction due to the (TZ,DZ) extrapolation. We estimate errors due to basis set incompleteness by forming the difference between 5Z and QZ calculations for H_2O–C_6H_6.

To assess the accuracy limits of the L-CCSD(T) method, we examine the convergence of the L-CCSD(T) energies with respect to the three main thresholds, namely, LoosePNO, NormalPNO, and TightPNO as defined in Ref. 106 by calculating interaction energies of the 0-, 1-, and 2-leg H_2O–C_6H_6 dimers using the cc-pVTZ, cc-pVQZ, and cc-pV5Z basis sets. The same analysis is also carried out for H_2O–$C_{24}H_{12}$ using the cc-pVTZ basis set. The results of this analysis are reported in the Tables S21 and S22 of the Supporting Information. In general, the differences in interaction energies calculated with the NormalPNO and TightPNO thresholds for the H_2O–C_6H_6 dimer in the CBS limit are within

∼0.2, ∼0.1, and ∼0.2 kcal/mol for 0-, 1-, and 2-leg configurations, respectively. Similar differences are found for the H_2O–$C_{24}H_{12}$ dimer using the cc-pVTZ basis set. Compared to canonical CCSD(T)/cc-pVTZ, L-CCSD (T)/cc-pVTZ calculations with the NormalPNO threshold slightly overestimate the interaction energy (by ∼0.1 kcal/mol for both 1- and 2-leg configurations and ∼0.2 kcal/mol for 0-leg configurations). Opposite trend is observed for L-CCSD(T))/cc-pVTZ calculations with the TightPNO threshold which are found to underestimate the interaction energy by ∼0.1 kcal/mol compared to the CCSD(T)/cc-pVTZ values. As shown in Table S22 in the Supporting Information, L-CCSD(T) calculations with the TightPNO threshold are significantly computationally more expensive than those carried out with the NormalPNO threshold. Considering the small differences in the interaction energies calculated with the two thresholds, the NormalPNO threshold is adopted in all L-CCSD(T) calculations presented in the following sections. We note that L-CCSD(T) calculations for water interacting with PAH molecules have recently been carried out, although only for the H_2O–$C_{24}H_{12}$ and H_2O–$C_{24}H_{12}$ dimers, using the TightPNO threshold and a different extrapolation procedure to account for basis-set incompleteness.[38] Comparisons between the present L-CCSD(T) results and those of Ref. 38 are shown in Section S6 of the Supporting Information. For both dimers, the differences between the interaction energies predicted by the two sets of L-CCSD(T) calculations never exceed 0.4 kcal/mol.

3   RESULTS

3.1   Interaction energies for water on C_6H_6, $C_{24}H_{12}$, and $C_{54}H_{18}$

Fig. 2 shows comparisons between potential energy curves calculated using GGA (top row), meta-GGA (middle row), and hybrid (bottom row) functionals for 0-leg (panels a-c), 1-leg (panels d-f), and 2-leg (panels g-i) configurations of the H_2O–C_6H_6 dimer, along with the corresponding RPA and L-CCSD(T) values. Also shown are the available DMC data from Ref. 38.

Figure 2: Comparison between DFT, RPA, and L-CCSD(T) interaction energies (in kcal/mol) calculated for 0-leg, 1-leg, and 2-leg configurations of H_2O–C_6H_6. Top panels: GGA functionals (red), middle panels: meta-GGA functionals (green), bottom panels: hybrid and range-separated hybrid, meta-GGA functionals (cyan). Also shown are the available DMC data from Ref. 38. The intermolecular distances (R) are defined as the vertical distances between the O atom of the water molecule and the plane of the C_6H_6 molecule.

Independently of the level of theoretical treatment, water in the 0-leg configuration is predicted not to be bound to C_6H_6, in agreement with previous studies.[15,107] Most GGA and meta-GGA functionals, with the exception of BLYP-D3 and revPBE-D3, predict interaction energies that are in good agreement (with deviations within $\sim$0.1 kcal/mol) with the corresponding L-CCSD(T) values for 0-leg intermolecular distances between 2.5 Å and 4.0 Å. In contrast, both BLYP-D3 and revPBE-D3 predict interaction energies similar to those obtained at the RPA level of theory, which, in turn, deviates by $\sim$0.4 kcal/mol from the corresponding L-CCSD(T) values for intermolecular distances between 2.5 Å and 4.0 Å. All hybrid functionals considered in this study predict interaction energies for 0-leg configurations of H_2O–C_6H_6 similar to those obtained with RPA. For 0-leg configurations, the DMC results of Ref. 38 are statistically indistinguishable from the present RPA values.

Both 1-leg and 2-leg configurations of water bind to C_6H_6, with RPA and L-CCSD(T) predicting interaction energies between 2.50 and 3.0 kcal/mol and between 2.80 and 3.20 kcal/mol for 1-leg and 2-leg minimum-energy configurations, respectively. While RPA tends to underestimate the interaction energies, with deviations of $\sim$0.5 kcal/mol from the corresponding L-CCSD(T) values for intermolecular distances between 2.5 Å and 4.0 Å, the available DMC results[38] are generally closer to the L-CCSD(T) values, underestimating the interaction energies by $\sim$0.2 kcal/mol. Among the GGA functionals considered in this study, BLYP-D3, revPBE-D3, and rVV10 systematically overestimate the interaction strength between 2.5 Å and 4.0 Å by 0.2–0.3 kcal/mol. Somewhat larger deviations (up to -0.70 kcal/mol) from the L-CCSD(T) values are associated with meta-GGA and hybrid functionals in the 1-leg and 2-leg energy minimum regions, with the exception of B97M-rV and ωB97M-V that closely reproduce the L-CCSD(T) curves at all H_2O–C_6H_6 separations.

As shown in Fig. 3, by increasing the size of the PAH molecule from C_6H_6 to $C_{24}H_{12}$, more defined trends in the interaction energies begin to emerge. First, contrary to C_6H_6, water is bound to coronene in the 0-leg configuration. Second, interaction energies calculated at different levels of theory become more distinct. For instance, the differences
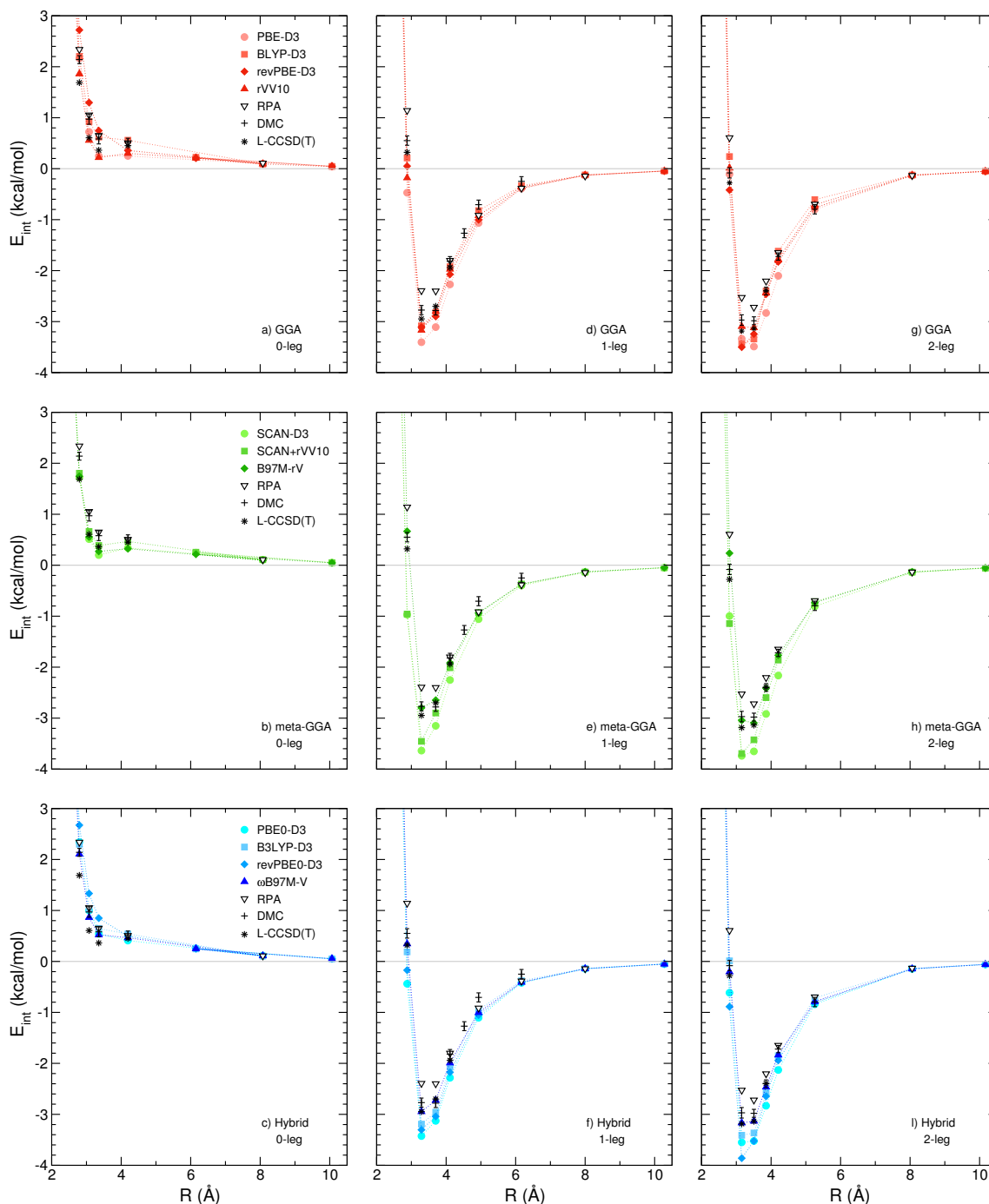
Figure 3: Comparison between DFT, RPA, and L-CCSD(T) interaction energies (in kcal/mol) calculated for 0-leg, 1-leg, and 2-leg configurations of H_2O–$C_{24}H_{12}$. Top panels: GGA functionals (red), middle panels: meta-GGA functionals (green), bottom panels: hybrid and range-separated hybrid, meta-GGA functionals (cyan). Also shown are the available DMC data from Ref. 38. The intermolecular distances (R) are defined as the vertical distances between the O atom of the water molecule and the plane of the $C_{24}H_{12}$ molecule.

between L-CCSD(T) and RPA interaction energies in the minimum energy region increase to 0.8 kcal/mol, 1.0 kcal/mol, and 0.9 kcal/mol for 0-leg, 1-leg, and 2-leg configurations, respectively. These results are in line with previous observations of RPA tending to underestimate interaction energies of dispersion-bound complexes.[108] Energy differences on the order of 0.2–0.4 kcal/mol are found between the present L-CCSD(T) interaction energies and the available DMC values[38] for all three orientations of water in the minimum energy region of the H_2O–$C_{24}H_{12}$ dimer. Overall, for all three orientations, L-CCSD(T) and RPA predict the strongest and weakest interactions, respectively, with the DMC values lying in between, in line with the results shown in Fig. 2 for the H_2O–C_6H_6 dimer.

Among the GGA functionals considered in this study, rVV10 predicts interaction energies for the H_2O–$C_{24}H_{12}$ dimer which are in relatively good agreement with the corresponding L-CCSD(T) values for 0-leg configurations but slightly underbinds and overbinds (by $\sim$0.1 kcal/mol) 1-leg and 2-leg configurations, respectively. All other GGA functionals tend to underestimate the interaction energy for 0-leg configurations while they overbind water to coronene in 1-leg and 2-leg configurations. Among the meta-GGA functionals, B97M-rV and SCAN-D3 reproduce the L-CCSD(T) interaction energies for 0-leg configurations, whereas SCAN+rVV10 underbinds the H_2O–$C_{24}H_{12}$ dimer by 0.3 kcal/mol. However, in the minimum region of both 1- and 2-leg configurations, SCAN-D3 overestimates the interaction energy by $\sim$0.6 kcal/mol contrary to B97M-rV and SCAN+rVV10 that provide good agreement with L-CCSD(T). The hybrid functionals exhibit similar trend as their GGA counterparts, systematically underestimating the interaction energies for 0-leg configurations while overbinding the H_2O–$C_{24}H_{12}$ dimer in both 1-leg and 2-leg configurations. Independently of the water orientation, ωB97M-V is consistently the best performing functional, closely reproducing the L-CCSD(T) values at all intermolecular distances.

As discussed in Section 2.4, due to the associated computational cost, L-CCSD(T) calculations for the H_2O–$C_{54}H_{18}$ dimer are only carried out at the cc-pVDZ and cc-pVTZ basis sets for configurations in the minimum energy region. Fig. 4 shows that the differences between
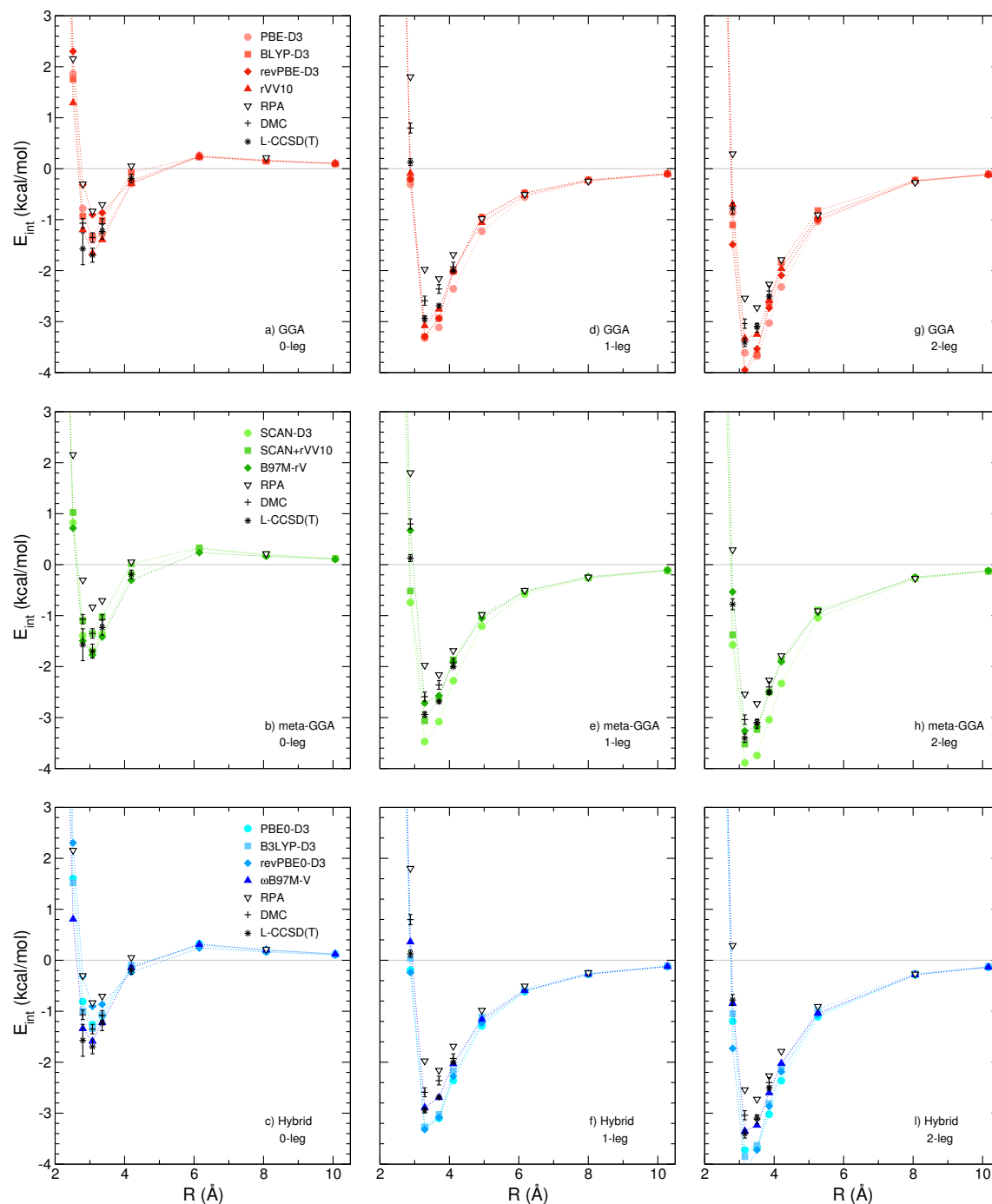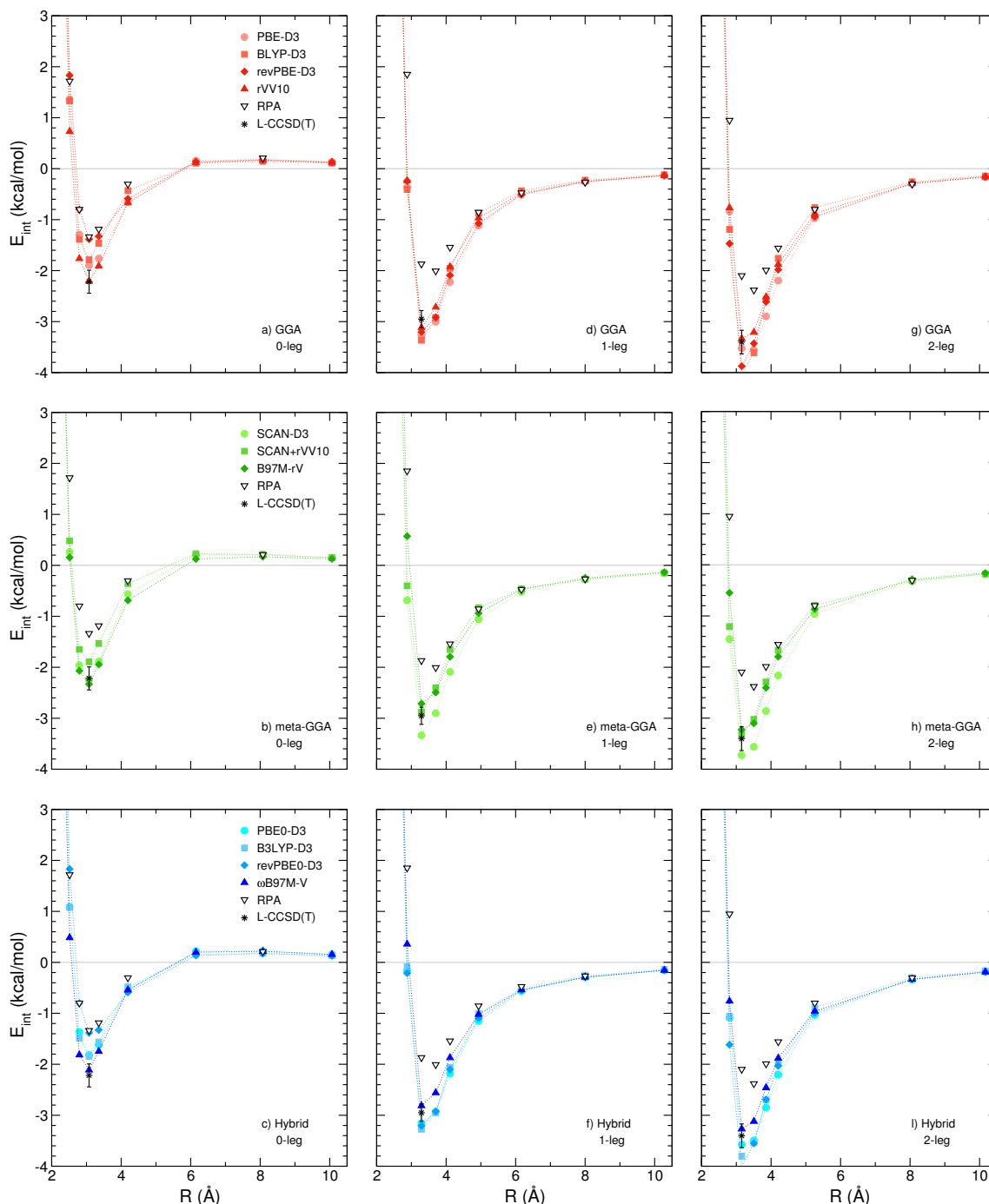
Figure 4: Comparison between DFT, RPA, and L-CCSD(T) interaction energies (in kcal/mol) calculated for 0-leg, 1-leg, and 2-leg configurations of H_2O–$C_{54}H_{18}$. Top panels: GGA functionals (red), middle panels: meta-GGA functionals (green), bottom panels: hybrid and range-separated hybrid, meta-GGA functionals (cyan). Also shown are the available DMC data from Ref. 38. The intermolecular distances (R) are defined as the vertical distances between the O atom of the water molecule and the plane of the $C_{54}H_{18}$ molecule.

RPA and L-CCSD(T) interaction energies are more pronounced than for the H_2O–C_6H_6 and H_2O–$C_{24}H_{12}$ dimers, being in the range of 0.8–1.0 kcal/mol for 0-leg configurations, 0.9–1.1 kcal/mol for 1-leg configurations, and 1.0–1.3 kcal/mol for 2-leg configurations. Among the different XC functionals, PBE-D3, rVV10, SCAN+rVV10, B97M-rV, and ωB97M-V predict interaction energies that are in better agreement with the L-CCSD(T) values.

In order to facilitate the comparison between various XC functionals and identify general trends, we limit the discussion to rVV10, B97M-rV, and ωB97M-V as representatives for the GGA, meta-GGA, and hybrid and range-separate hybrid, meta-GGA functionals, respectively. As shown in Fig. 4, independently of the water orientation, the differences between rVV10 and L-CCSD(T) interaction energies in the minimum energy regions do not exceed 0.2 kcal/mol, while both B97M-rV and ωB97M-V predict interaction energies that lie within the uncertainties associated with the corresponding L-CCSD(T) values. The comparisons shown in Figs. 2–3 indicate that the differences between RPA and L-CCSD(T) interaction energies calculated for the H_2O–C_6H_6, H_2O–$C_{24}H_{12}$, and H_2O–$C_{54}H_{18}$ dimers increase as a function of the PAH molecule size, with RPA systematically underbinding all three dimers, independently of the water orientation. Although less pronounced, similar trend is also observed for the differences between the present L-CCSD(T) results and the DMC data available for the H_2O–C_6H_6 and H_2O–$C_{24}H_{12}$ dimers. On the other hand, most XC functionals examined in this study tend to underbind 0-leg configurations and overbind 1-leg and 2-leg configurations. As a result of this general trend, GGA functionals overestimate the relative stability of 1-leg and 2-leg configurations relative to 0-leg configurations, while, among all XC functionals considered in this study, B97M-rV and ωB97M-V are the best performing functionals in representing the energetics of all three water–PAH dimers shown in Figs. 2–3. In particular, independently of the water orientation, ωB97M-V is found to reproduce, nearly quantitatively, the corresponding L-CCSD(T) values.

Additional insights into the nature of water–PAHs interactions can be gained from calculations carried out using the absolutely localized molecular orbital energy decomposition
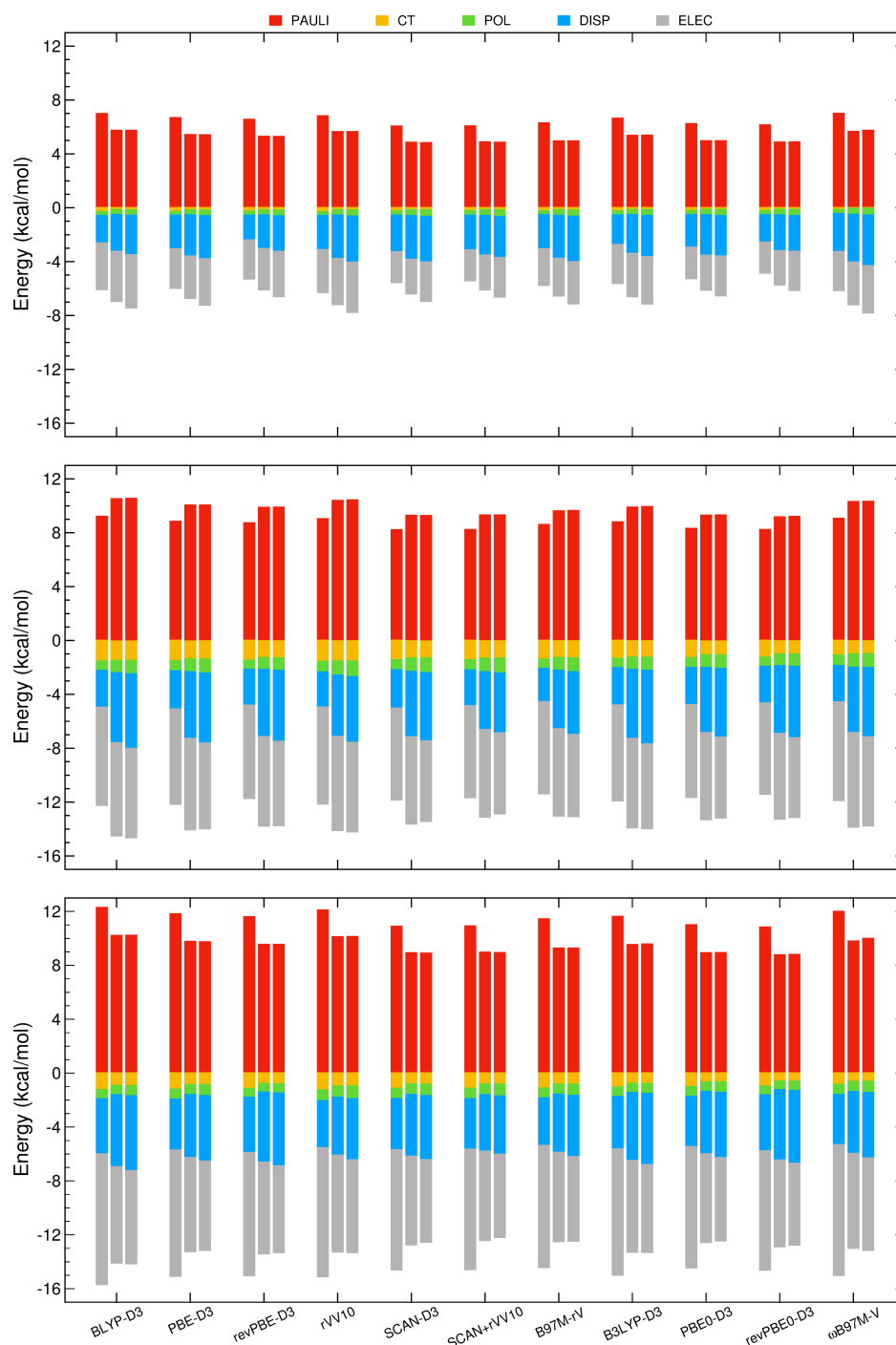
Figure 5: ALMO-EDA results for H_2O–C_6H_6 (top), H_2O–$C_{24}H_{12}$ (middle), and H_2O–$C_{54}H_{18}$ (bottom) dimers. On the vertical axes are the energies, in kcal/mol, of each component of the interaction energy. Each group of bars from left to right corresponds to 0-leg, 1-leg, and 2-leg configurations. Color scheme: PAULI in red, CT in yellow, POL in green, DISP in blue, ELECT in gray. See main text for details.

analysis (ALMO-EDA) method.[66,67] ALMO-EDA separates the intermolecular interaction energy into Pauli repulsion (PAULI), permanent electrostatics (ELEC), polarization (POL), dispersion energy (DISP), and charge transfer (CT) contributions. Fig. 5 shows that there is no qualitative difference in the way various XC functionals considered in this study represents the individual contributions to the interaction energies. In addition, no qualitative differences exist as a function of water orientation and number of carbon atoms in the PAH molecules. We can then conclude that the purely repulsive nature of the H_2O–C_6H_6 interaction in the 0-leg configuration is a consequence of the dominant role played by the Pauli repulsion term, outweighing the combined attractive contributions from all other energy components. It should be noted that the Pauli repulsion term associated with the 0-leg configuration is not as repulsive as in the 1-leg and 2-leg configurations (top, middle, and bottom panels of Fig. 5) for which the closer approach of the water hydrogen atom(s) initiates overlap of atomic orbitals with the benzene π system. In spite of the increase in Pauli repulsion for 1-leg and 2-leg configurations, the corresponding interaction energies are negative due to counterbalancing effects associated with the ELEC, POL, DISP, and CT terms, with ELEC representing the dominant contribution, in line with previous analyses of molecular complexes characterized by lone pair–π-electron interactions.[107]

Going from H_2O–C_6H_6 to H_2O–$C_{24}H_{12}$, the PAULI contribution to the 0-leg interaction energy becomes significantly less repulsive, while the POL, DISP, and ELEC terms become relatively more attractive, and the CT term remains effectively unchanged. Compared to the ALMO-EDA results for 1-leg and 2-leg configurations of the H_2O–C_6H_6 dimer, the DISP term becomes more attractive, while both CT and ELEC contributions to the interaction energies become less attractive, with ELEC still representing the dominant contribution. Finally, no appreciable differences in the relative contributions to the interaction energies are found between the H_2O–$C_{24}H_{12}$ and H_2O–$C_{54}H_{18}$ dimers.

3.2   H$_2$O interactions with larger PAH molecules, from C$_{96}$H$_{24}$ to C$_{216}$H$_{36}$

Owing to the good performance of B97M-rV and ωB97M-V in describing the H$_2$O–C$_6$H$_6$, H$_2$O–C$_{24}$H$_{12}$, and H$_2$O–C$_{54}$H$_{18}$ dimers discussed in Section 3.1, both functionals are used to investigate the dependence of the water–PAH interaction energies on the number of carbon atoms in larger PAH molecules for which RPA and L-CCSD(T) calculations become significantly more expensive. Specifically, continuing on the series of symmetric PAH molecules, interaction energies are calculated for 0-leg, 1-leg, and 2-leg configurations of the H$_2$O–C$_{96}$H$_{24}$, H$_2$O–C$_{150}$H$_{30}$, and H$_2$O–C$_{216}$H$_{36}$ dimers.

The evolution of the B97M-rV and ωB97M-V interaction energies from the H$_2$O–C$_6$H$_6$ to the H$_2$O–C$_{216}$H$_{36}$ dimer are shown in the top and bottom panels of Fig. 6, respectively. Both functionals predict that the strength of water–PAH interactions for 0-leg configurations increases monotonically with the number of carbon atoms. In the case of 1-leg and 2-leg configurations, the trend is reversed, with the H$_2$O–C$_6$H$_6$ dimer displaying the largest interaction energy among the PAH series. Importantly, while water in the 2-leg configuration is predicted to always interact more strongly with the PAH molecules, independently of the number of carbon atoms, both functionals predict a crossover in the interaction energies associated with 0-leg and 1-leg configurations which occurs between H$_2$O–C$_{150}$H$_{30}$ and H$_2$O–C$_{216}$H$_{36}$, with the 0-leg configuration becoming more attractive than the 1-leg configuration by $\sim$0.02 kcal/mol.

Building on the analysis presented in Section 3.1, ALMO-EDA calculations carried out for 0-leg, 1-leg, and 2-leg configurations in the minimum energy regions (Fig. 7) indicate that there is no qualitative difference in the relative magnitude of the different terms predicted by the B97M-rV and ωB97M-V functionals. According to the ALMO-EDA results, polarization and charge transfer terms do not contribute substantially to the total interaction energy and remain approximately constant, independently of the size of the PAH molecule. On the other hand, by counteracting the positive contribution due to Pauli repulsion, the dispersion

energy and electrostatic terms are effectively responsible for the attractive nature of the water–PAH interactions. Importantly, both these terms also exhibit the slowest convergence with the number of carbon atoms. In particular, while the dispersion energy term becomes more negative from C_6H_6 to $C_{216}H_{36}$ for all three water orientations, the variation of the

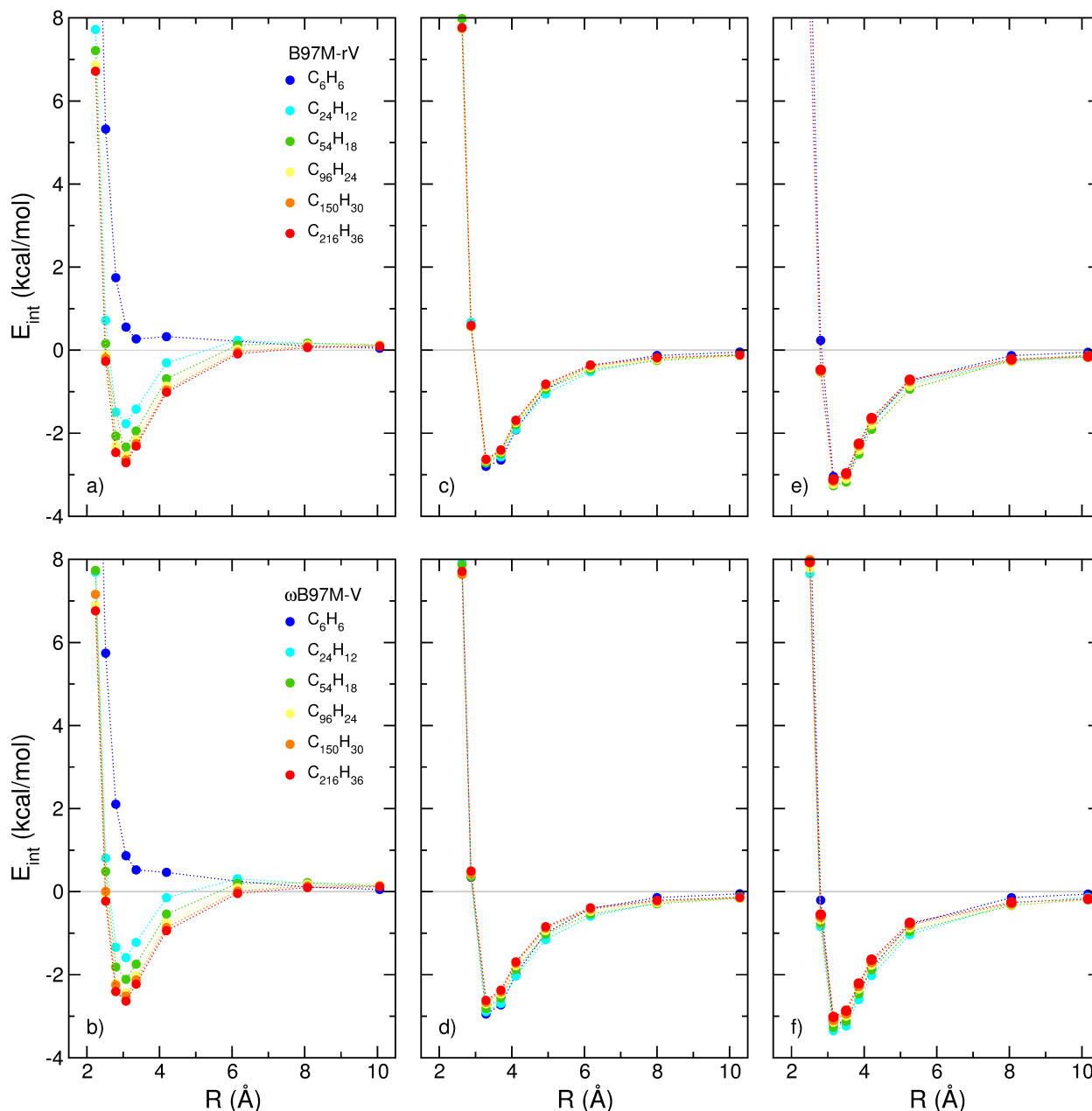Figure 6: B97M-rV (top panels) and ωB97M-V (bottom panels) interaction energy curves calculated for 0-leg (a and b), 1-leg (c and d), and 2-leg (e and f) configurations of all H_2O–PAH dimers examined in this study. See main text for details.
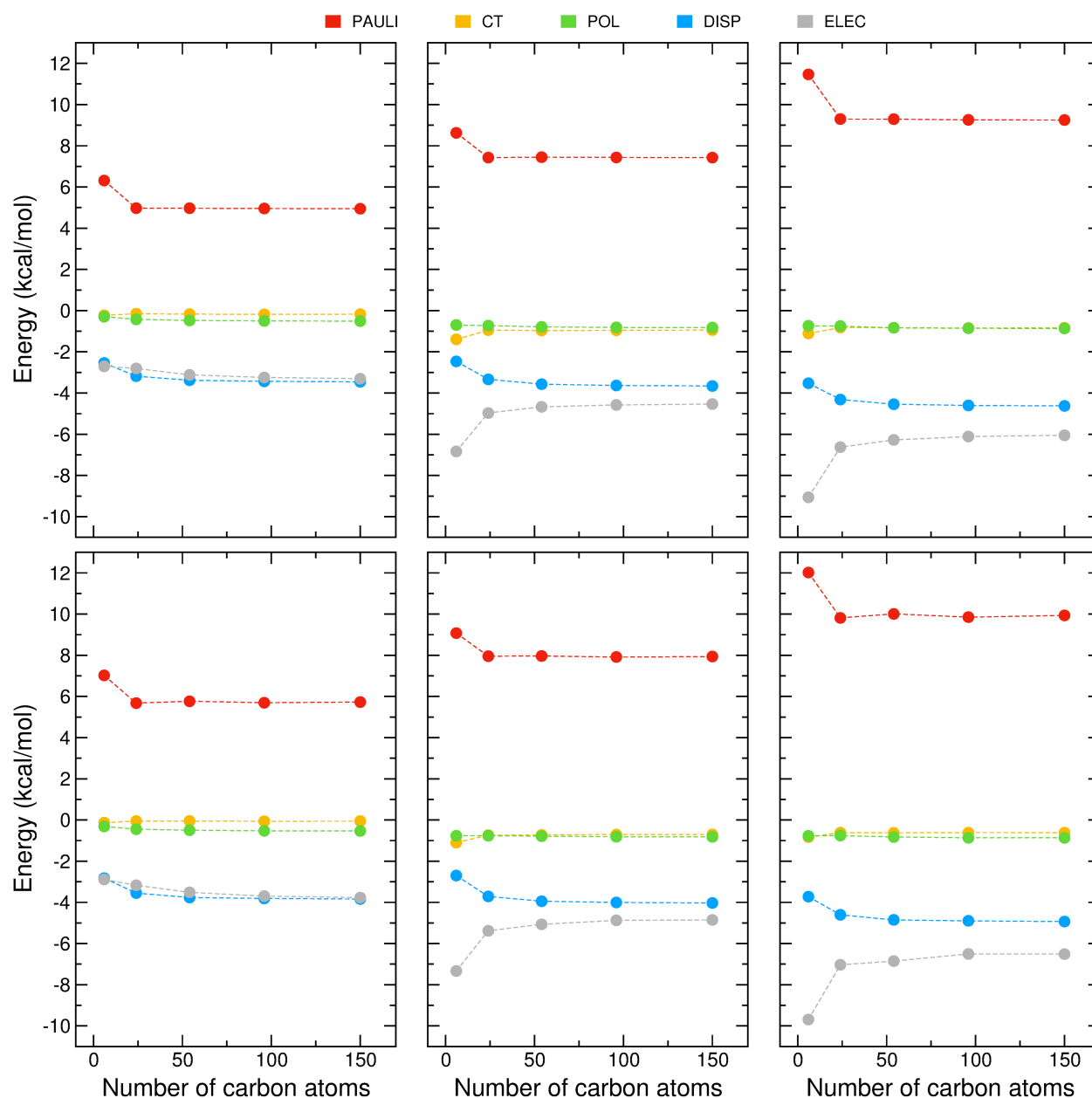
Figure 7: Decomposition of the total intermolecular interaction energy of water–PAH system as predicted by the B97M-rV (top) and ωB97M-V (bottom) functionals. On the vertical axis are the energies, in kcal/mol, of the energy components and the horizontal axis represents the system size as defined by the 0-leg, 1-leg, and 2-leg configurations. Color scheme: PAULI in red, CT in yellow, POL in green, DISP in blue, ELECT in gray. See main text for details.

electrostatic contributions depends on the water orientation, increasing in magnitude for 0-leg

configurationw while decreasing for both 1-leg and 2-leg configurations as the size of the PAH

molecules increases. The different dependence of the ELEC term on the water orientation

thus appears to be responsible for the crossover between 0-leg and 1-leg interaction energies occurring in Fig. 6 between H_2O–$C_{150}H_{30}$ and H_2O–$C_{216}H_{36}$. The analysis of the electrostatic properties of the different dimers shows that the Q_{zz} component of quadrupole moment of the PAH molecules becomes increasingly negative as a function of number of carbon atoms. This trend is rationalized by considering that carbon atoms in aromatic rings exhibit a permanent quadrupole moment due to the distribution of π electrons above and below the plane of the PAH molecule.[109]

3.3 H_2O interactions with graphene

Having characterized the magnitude and nature of the interactions between water and PAH molecules from C_6H_6 to $C_{216}H_{36}$, and assessed the performance of various XC functionals, in this section we examine the interaction of water with graphene. Due to the computational cost associated with hybrid functionals, the analysis will be limited to GGA and meta-GGA functionals. Based on the good performance exhibited by B97M-rV in describing the interactions between water and PAH molecules, we first show in Fig. 8 the 0-leg, 1-leg, and 2-leg interaction energy curves calculated with B97M-rV for the H_2O on graphene. Also shown in Fig. 8 are the available RPA and DMC data reported in Ref. 38. As mentioned in the Introduction, previous DMC calculations predicted significantly smaller (by ∼0.6 kcal/mol) interaction energies for both 1-leg and 2-leg configurations of water on graphene than those reported in Ref. 38.

Focusing on the minimum energy regions for the three different water orientations, it is possible to see that the RPA and DMC results of Ref. 38 are in agreement for 0-leg configurations while differences of ∼0.4 kcal/mol are found for both 1-leg and 2-leg configurations. These differences are similar to those found for the H_2O–C_6H_6 and H_2O–$C_{24}H_{12}$ dimers in Figs. 2 and 3 which also show that noticeable differences exist between RPA, DMC, and L-CCSD(T) interaction energies, particularly for 1-leg and 2-leg configurations. On the other hand, independently of the water orientation, B97M-rV predicts stronger water–graphene
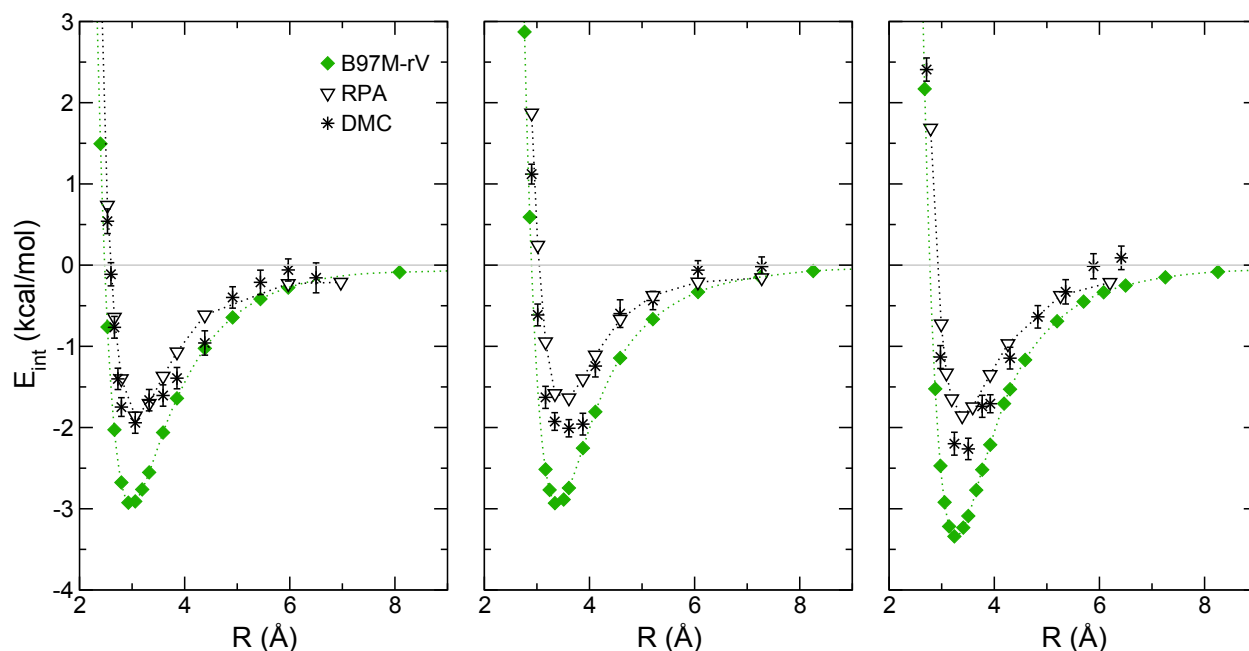
Figure 8: Interaction energy curves for the 0-leg (left), 1-leg (middle), and 2-leg (right) of all H_2O–graphene dimer resulting from the B97M-rV calculations. Also shown are the corresponding DMC and RPA data taken from Ref. 38.

interactions than both RPA and DMC, with differences up to -1.7 kcal/mol and -1 kcal/mol, respectively. These results are in line with the differences between RPA, DMC, and B97M-rV interaction energies calculated in Figs. 2–4 going from H_2O–C_6H_6 to H_2O–$C_{54}H_{18}$. In this context, it should be noted that B97M-rV closely reproduces the L-CCSD(T) interaction energies for H_2O–C_6H_6, H_2O–$C_{24}H_{12}$, and H_2O–$C_{54}H_{18}$ dimers.

Additional insights into the variation of the strength and anisotropy of water–PAH interactions from H_2O–C_6H_6 to H_2O–graphene are gained from the comparisons shown in Fig. 9 between interaction energies calculated using the same set of XC functionals examined in the previous sections. To facilitate the analysis of water–PAH interaction energies as a function of the number of carbon atoms in the PAH molecules, the comparisons are made for intermolecular distances of 3.075 Å, 3.289 Å, and 3.155 Å, corresponding to the minimum energy regions for 0-leg, 1-leg, and 2-leg configurations, respectively. General trends can be established for 0-leg interaction energies calculated with the different XCn functionals. In particular, as the size of the PAH molecules increases up to $C_{216}H_{36}$, the interaction

energies predicted by rVV10, SCAN-D3, B97M-rV, and ωB97M-V effectively converge to the same value of approximately -2.6 kcal/mol. Similarly, PBE-D3, SCAN-rVV10, B3LYP-D3, and PBE0-D3 interaction energies converge to approximately -2.2 kcal/mol. Among all functionals considered in this study, revPBE-D3 predicts the weakest water–PAH interactions for 0-leg configurations. In contrast, no common convergence behavior is predicted by the different functionals for both 1-leg and 2-leg configurations, with spreads of up to $\sim$2 kcal/mol. As discussed in Sections 3.1–3.2, B97M-rV and ωB97M-V provide nearly identical results from C_6H_6 to $C_{216}H_{36}$, closely reproducing the L-CCSD(T) results for water interacting with the smallest PAH molecules. Importantly, both revPBE-D3 and B3LYP-D3 predict an increase in the interaction strength for 1-leg configurations from water–benzene
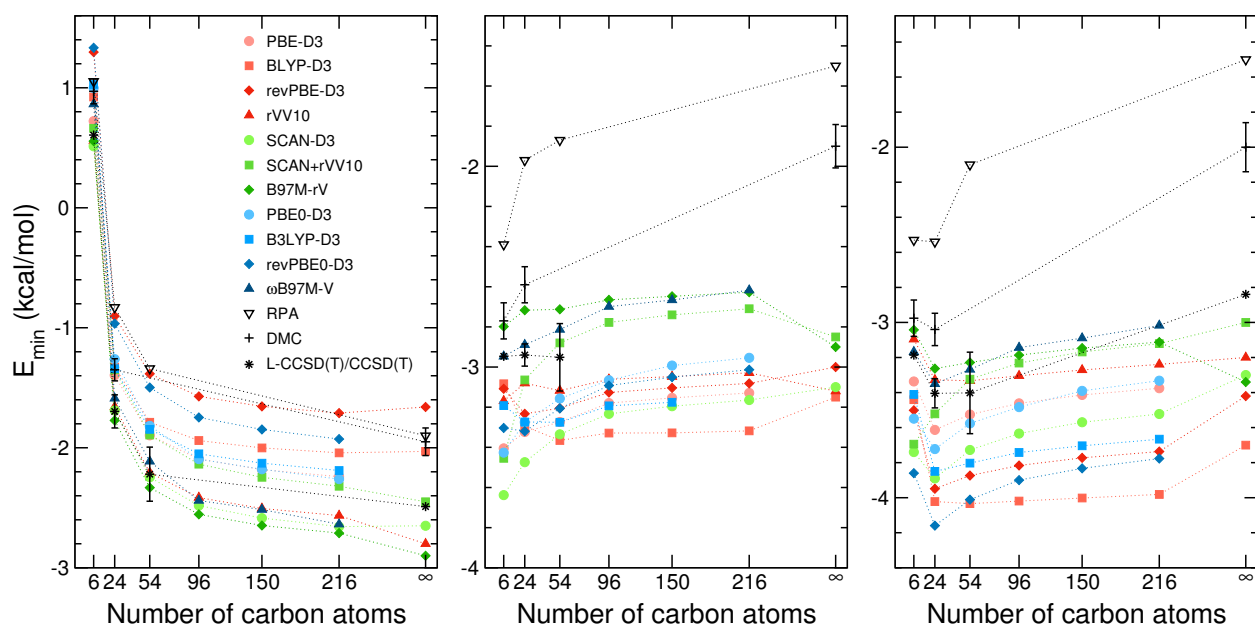
Figure 9: Water-PAH interaction energies calculated as a function of the number of carbon atoms in the PAH molecules. The intermolecular separation between the O atom of H_2O and the PAH molecules is fixed at 3.075 Å, 3.289 Å, and 3.155 Å defining the 0-leg, 1-leg, and 2-leg configurations. RPA and DMC water–graphene values taken from Ref. 38 are interpolated. The CCSD(T) data for water–graphene are taken from Ref. 39 and were obtained using a different setup from the present L-CCSD(T) calculations. Specifically, the CCSD(T) calculations were carried out for a 3×3 graphene supercells, using the cc-pVDZ and aug-cc-pVTZ basis sets for the C and H atoms of graphene, and the O and H atoms of the water molecule, respectively. In all panels, the dashed lines do not correspond to actual data but are only used as guides to the eye.

to water–coronene, which is opposite to the trend predicted by the L-CCSD(T) calculations. For 2-leg configurations, RPA predicts nearly identical interaction energies for both C_6H_6 and $C_{24}H_{12}$, which is similar to the trend observed in the DMC analysis reported in Ref. 38, while L-CCSD(T) predicts a decrease of $\sim$0.4 kcal/mol between the two dimers. Most XC functionals considered in this study exhibit, at least qualitatively, the same trend as L-CCSD(T), predicting a decrease in the interaction energy from benzene to coronene, which is followed by a steady increase as the number of carbon atoms increases up to $C_{216}H_{36}$. Notable exception is SCAN+rVV10 that predicts a monotonic increase of the interaction energies from C_6H_6 to $C_{216}H_{36}$. In general, B97M-rV and ωB97M-V provide the strongest interactions for 0-leg configurations, while predicting the weakest interactions for 1-leg and 2-leg configurations. Opposite trend is predicted by BLYP-D3, revPBE-D3, B3LYP-D3, and revPEB0-D3, while SCAN-D3 overall predicts the strongest interactions, independently of the water orientations.

Fig. 9 also shows comparisons of water–graphene interaction energies calculated with GGA and meta-GGA functionals with the available RPA and DMC data.[38] The corresponding CCSD(T) calculations[39] carried out with the cc-pVDZ/aug-cc-pVTZ basis sets place the water–graphene interaction at -2.49 (0-leg) and -2.84 kcal/mol (2-leg). It should be noted that, due the relatively small basis set used in these calculations, these results may suffer from non-negligible errors due to basis set incompleteness. In addition, while CCSD(T) is considered highly accurate for large-gap molecular compounds and insulators, the perturbative triples correction diverges for bulk graphene, and further validation of the available CCSD(T) values using non-perturbative approaches is desirable. For 0-leg configurations in the minimum energy region, BLYP-D3 reproduces the RPA and DMC results, while SCAN+rVV10 data is in good agreement with the CCSD(T) value, which lie $\sim$0.5 kcal/mol below. Compared to CCSD(T), GGA functionals, with the exception of rVV10, tend to underestimate the interaction energy for 0-leg configurations, while meta-GGA functionals, with the exception of B97M-rV, provide closer agreement with the CCSD(T) values. Unfor-

26

tunately, due to the associated computational cost, no data are available for water–graphene interactions calculated with hybrid functionals.

Most XC functionals predict significant variations in the interaction energy for 1-leg and 2-leg configurations relative to the largest PAH molecule ($C_{216}H_{36}$) considered in this study. Specifically, BLYP-D3, revPBE-D3, and SCAN-D3 predict interaction energies for 1-leg water–graphene configurations that are $\sim$0.1-0.3 kcal/mol smaller than for the corresponding H_2O–$C_{216}H_{36}$ configurations, while opposite trends are observed for rVV10, SCAN+rVV10, and B97M-rV, which all predict stronger interactions for water on graphene. On the other hand, with the exception of B97M-rV, all GGA and meta-GGA functionals examined in this study predict a decrease in the interaction strength for 2-leg configurations going from H_2O–$C_{216}H_{36}$ to water–graphene, although the extent of this decrease varies significantly among the different XC functionals. These large variations in interaction energies from PAH molecules to graphene may be ascribed to basis set incompleteness errors in the water–graphene calculations which, directly modulating the extent of charge transfer, polarization, and electrostatic effects (Figs. 5 and 7), can affect differently the interaction strength of different water orientations. Both GGA and meta-GGA functionals predict interaction energies for water–graphene 1-leg and 2-leg configurations that are closer to the CCSD(T) values than to the corresponding RPA and DMC data. Among the different XC functionals examined in this study, SCAN+rVV10 provides the best agreement with the CCSD(T) results, with deviations of $\sim$0.2 kcal/mol. Relatively larger deviations, between 0.4–0.9 kcal/mol, are associated with the other GGA and meta-GGA functionals. These results seem to be in line with previous observations on the performance of different XC functionals in describing the properties of water on boron nitride.[63]

4　CONCLUSIONS

We have reported a systematic analysis of the interaction energies between a single water molecule and a series of PAH molecules, from benzene to graphene, using various XC functionals representative of the GGA, meta-GGA, hybrid, and range-separated hybrid, meta-GGA families. The accuracy of the different functionals has been assessed through direct comparisons with the corresponding values obtained at the RPA and L-CCSD(T) levels of theory as well as with available DMC data reported in the literature.[38] In this analysis, three orientations of the water molecule relative to the plane of the PAH molecules are considered, corresponding to configurations with the oxygen atom of the water molecule pointing perpendicular to the center of the PAH molecules (0-leg configurations), one hydrogen of the water molecule pointing perpendicular to one carbon atom of the central ring of the PAH molecules (1-leg configurations), and both hydrogen atoms pointing to the plane of the PAH molecules (2-leg configurations).

Relatively large variability is found in the ability of different XC functionals to describe water–PAH interactions, independently of the water orientation. In particular, it is found that GGA functionals tend to underestimate the interaction strength for 0-leg configurations, while they overestimate the interaction strength for both 1-leg and 2-leg configurations. Overall, the meta-GGA B97M-rV and range-separated hybrid, meta-GGA ωB97M-V functionals provide nearly quantitative agreement with L-CCSD(T) values available for H_2O–C_6H_6, H_2O–$C_{24}H_{12}$, and H_2O–$C_{54}H_{18}$. Similar trends among GGA, meta-GGA, and hybrid functionals are observed for the larger PAH molecules (up to $C_{216}H_{36}$) for which no RPA, DMC, and L-CCSD(T) reference data are currently available. Further insights into the nature of water–PAH interactions are gained from ALMO-EDA calculations, which show that, independently of the number of carbon atoms and exchange-correlation functional, electrostatic and dispersion interactions represent the largest contributions, while polarization and charge transfer effects are negligibly small.

Finally, calculations carried out with GGA and meta-GGA functionals indicate that,

as the number of carbon atoms increases, the interaction energies slowly converge to the corresponding values obtained for an infinite graphene sheet. Deviations up to ~ 1.5 kcal/mol are found among RPA, DMC, and CCSD(T) values reported in the literature for water–graphene interactions which, while highlighting the difficulties associated with converging high-level electronic structure calculations in periodic boundary conditions in terms of basis-set size and finite-size effects, makes it difficult to quantitatively and unambiguously assess the accuracy of different XC functionals.

Acknowledgement

References

(1) Feller, D.; Jordan, K. D. Estimating the Strength of the Water/Single-Layer Graphite Interaction. *J. Phys. Chem. A* **2000**, *104*, 9971–9975.

(2) Koga, K.; Gao, G.; Tanaka, H.; Zeng, X. C. Formation of Ordered Ice Nanotubes Inside Carbon Nanotubes. *Nature* **2001**, *412*, 802–805.

(3) Werder, T.; Walther, J. H.; Jaffe, R. L.; Halicioglu, T.; Noca, F.; Koumoutsakos, P. Molecular Dynamics Simulation of Contact Angles of Water Droplets in Carbon Nanotubes. *Nano Letters* **2001**, *1*, 697–702.

(4) Hummer, G.; Rasaiah, J. C.; Noworyta, J. P. Water Conduction through the Hydrophobic Channel of a Carbon Nanotube. *Nature* **2001**, *414*, 188–190.

(5) Zhao, X.; Johnson, J. K. An Effective Potential for Adsorption of Polar Molecules on Graphite. *Mol. Simul.* **2005**, *31*, 1–10.

(6) Bushuev, Y.; Davletbaeva, S.; Muguet, F. F. Hydration Simulations of a Carbon Nanotube, Immersed in Water, According to the 3-Atractor Water Model. *Sensors* **2005**, *5*, 139–147.

(7) Pertsin, A.; Grunze, M. Water as a Lubricant for Graphite: A Computer Simulation Study. *J. Chem. Phys.* **2006**, *125*, 114707.

(8) Thomas, J.; McGaughey, A. Effect of Surface Wettability on Liquid Density, Structure, and Diffusion Near a Solid Surface. *J. Chem. Phys.* **2007**, *126*, 034707.

(9) Birkett, G.; Do, D. Simulation Study of Water Adsorption on Carbon Black: The Effect of Graphite Water Interaction Strength. *J. Phys. Chem. C* **2007**, *111*, 5735–5742.

(10) González, B.; Hernández-Rojas, J.; Bretón, J.; Gomez Llorente, J. Global Potential Energy Minima of $(H_2O)_n$ Clusters on Graphite. *J. Phys. Chem. C* **2007**, *111*, 14862–14869.

(11) Thomas, J.; McGaughey, A. Density, Distribution, and Orientation of Water Molecules Inside and Outside Carbon Nanotubes. *J. Chem. Phys.* **2008**, *128*, 084715.

(12) Wehling, T. O.; Lichtenstein, A. I.; Katsnelson, M. I. First-Principles Studies of Water Adsorption on Graphene: The Role of the Substrate. *Appl. Phys. Lett.* **2008**, *93*, 202110.

(13) Leenaerts, O.; Partoens, B.; Peeters, F. Adsorption of H_2O, NH_3, CO, NO_2, and NO on Graphene: A First-Principles Study. *Phys. Rev. B* **2008**, *77*, 125416.

(14) Köfinger, J.; Hummer, G.; Dellago, C. Macroscopically Ordered Water in Nanopores. *Proc. Natl. Acad. Sci. U.S.A.* **2008**, *105*, 13218–13222.

(15) Rubes, M.; Nachtigall, P.; Vondrasek, J.; Bludsky, O. Structure and Stability of the Water-Graphite Complexes. *J. Phys. Chem. C* **2009**, *113*, 8412–8419.

(16) Jenness, G. R.; Jordan, K. D. DF-DFT-SAPT Investigation of the Interaction of a Water Molecule to Coronene and Dodecabenzocoronene: Implications for the Water-Graphite Interaction. *J. Phys. Chem. C* **2009**, *113*, 10242–10248.

(17) Jenness, G. R.; Karalti, O.; Jordan, K. D. Benchmark Calculations of Water–Acene Interaction Energies: Extrapolation to the Water–Graphene Limit and Assessment of Dispersion–Corrected DFT Methods. *Phys. Chem. Chem. Phys.* **2010**, *12*, 6375–6381.

(18) Hamada, I. Adsorption of Water on Graphene: A van der Waals Density Functional Study. *Phys. Rev. B* **2012**, *86*, 195436.

(19) Werder, T.; Walther, J. H.; Jaffe, R.; Halicioglu, T.; Koumoutsakos, P. On the Water-Carbon Interaction for Use in Molecular Dynamics Simulations of Graphite and Carbon Nanotubes. *J. Phys. Chem. B* **2003**, *107*, 1345–1352.

(20) Ho, T. A.; Striolo, A. Polarizability Effects in Molecular Dynamics Simulations of the Graphene-Water Interface. *J. Chem. Phys.* **2013**, *138*, 054117.

(21) Strong, S. E.; Eaves, J. D. Atomistic Hydrodynamics and the Dynamical Hydrophobic Effect in Porous Graphene. *J. Phys. Chem. Lett.* **2016**, *7*, 1907–1912.

(22) Jorgensen, W. L.; Chandrasekhar, J.; Madura, J. D.; Impey, R. W.; Klein, M. L. Comparison of Simple Potential Functions for Simulating Liquid Water. *J. Chem. Phys.* **1983**, *79*, 926–935.

(23) Cohen-Tanugi, D.; Grossman, J. C. Water Desalination across Nanoporous Graphene. *Nano Lett.* **2012**, *12*, 3602–3608.

(24) Konatham, D.; Yu, J.; Ho, T. A.; Striolo, A. Simulation Insights for Graphene-Based Water Desalination Membranes. *Langmuir* **2013**, *29*, 11884–11897.

(25) Cohen-Tanugi, D.; Lin, L.-C.; Grossman, J. C. Multilayer Nanoporous Graphene Membranes for Water Desalination. *Nano Lett.* **2016**, *16*, 1027–1033.

(26) Antony, J.; Grimme, S. Structures and Interaction Energies of Stacked Graphene–Nucleobase Complexes. *Phys. Chem. Chem. Phys.* **2008**, *10*, 2722–2729.

(27) Van Mourik, T.; Gdanitz, R. J. A Critical Note on Density Functional Theory Studies on Rare-gas Dimers. *J. Chem. Phys.* **2002**, *116*, 9620–9623.

(28) Cybulski, S. M.; Seversen, C. E. An Interaction Energy Decomposition Approach for the Supermolecule Density Functional Theory Calculations. *J. Chem. Phys.* **2003**, *119*, 12704–12707.

(29) Zhao, Y.; Truhlar, D. G. Benchmark Databases for Nonbonded Interactions and their use to Test Density Functional Theory. *J. Chem. Theory Comput.* **2005**, *1*, 415–432.

(30) Goerigk, L.; Hansen, A.; Bauer, C.; Ehrlich, S.; Najibi, A.; Grimme, S. A Look at the Density Functional Theory Zoo with the Advanced GMTKN55 Database for General Main Group Thermochemistry, Kinetics and Noncovalent Interactions. *Phys. Chem. Chem. Phys.* **2017**, *19*, 32184–32215.

(31) Grimme, S. Semiempirical Hybrid Density Functional with Perturbative Second-Order Correlation. *J. Chem. Phys.* **2006**, *124*, 034108.

(32) Grimme, S.; Antony, J.; Ehrlich, S.; Krieg, H. A Consistent and Accurate Ab Initio Parametrization of Density Functional Dispersion Correction (DFT-D) for the 94 Elements H-Pu. *J. Chem. Phys.* **2010**, *132*, 154104.

(33) Vydrov, O. A.; Van Voorhis, T. Nonlocal van der Waals Density Functional: The Simpler the Better. *J. Chem. Phys.* **2010**, *133*, 244103.

(34) Grimme, S.; Hansen, A.; Brandenburg, J. G.; Bannwarth, C. Dispersion-Corrected Mean-Field Electronic Structure Methods. *Chem. Rev.* **2016**, *116*, 5105–5154.

(35) Dion, M.; Rydberg, H.; Schröder, E.; Langreth, D. C.; Lundqvist, B. I. Van der Waals Density Functional for General Geometries. *Phys. Rev. Lett.* **2004**, *92*, 246401.

(36) Lee, K.; Murray, É. D.; Kong, L.; Lundqvist, B. I.; Langreth, D. C. Higher-accuracy van der Waals Density Functional. *Phys. Rev. B* **2010**, *82*, 081101.

(37) Ma, J.; Michaelides, A.; Alfe, D.; Schimka, L.; Kresse, G.; Wang, E. Adsorption and Diffusion of Water on Graphene from First Principles. *Phys. Rev. B* **2011**, *84*, 033402.

(38) Brandenburg, J. G.; Zen, A.; Fitzner, M.; Ramberger, B.; Kresse, G.; Tsatsoulis, T.; Grüneis, A.; Michaelides, A.; Alfè, D. On the Physisorption of Water on Graphene: Sub-chemical Accuracy from Many-body Electronic Structure Methods. *J. Phys. Chem. Lett.* **2019**, *10*, 358–368.

(39) Voloshina, E.; Usvyat, D.; Schütz, M.; Dedkov, Y.; Paulus, B. On the Physisorption of Water on Graphene: a CCSD(T) Study. *Phys. Chem. Chem. Phys.* **2011**, *13*, 12041–12047.

(40) Paulus, B. The Method of Incrementsa Wavefunction-Based Ab Initio Correlation Method for Solids. *Physics Reports* **2006**, *428*, 1–52.

(41) Rezac, J.; Hobza, P. Describing Noncovalent Interactions beyond the Common Approximations: How Accurate is the Gold Standard, CCSD(T) at the Complete Basis Set Limit? *J. Chem. Theory Comput.* **2013**, *9*, 2151–2155.

(42) Nozieres, P.; Pines, D. Correlation Energy of a Free Electron Gas. *Phys. Rev.* **1958**, *111*, 442–454.

(43) Langreth, D. C.; Perdew, J. P. Exchange-Correlation Energy of a Metallic Surface: Wave-Vector Analysis. *Phys. Rev. B* **1977**, *15*, 2884–2901.

(44) Dobson, J. In *Time-Dependent Density Functional Theory*; Marques, M. A., Ullrich, C. A., Nogueira, F., Rubio, A., Burke, K., Gross, E. K. U., Eds.; Springer Berlin Heidelberg: Berlin, Heidelberg, 2006; pp 443–462.

(45) Harl, J.; Kresse, G. Cohesive Energy Curves for Noble Gas Solids Calculated by Adiabatic Connection Fluctuation-Dissipation Theory. *Phys. Rev. B* **2008**, *77*, 045136.

(46) Harl, J.; Kresse, G. Accurate Bulk Properties from Approximate Many-Body Techniques. *Phys. Rev. Lett.* **2009**, *103*, 056401.

(47) Eshuis, H.; Furche, F. A Parameter-Free Density Functional That Works for Noncovalent Interactions. *The Journal of Physical Chemistry Letters* **2011**, *2*, 983–989.

(48) Wilhelm, J. Large-Scale Cubic-Scaling Random Phase Approximation Correlation Energy Calculations using a Gaussian Basis. *J. Chem. Theory Comput.* **2016**, *12*, 5851–5859.

(49) Chen, G. P.; Voora, V. K.; Agee, M. M.; Balasubramani, S. G.; Furche, F. Random-phase Approximation Methods. *Ann. Rev. Phys. Chem.* **2017**, *68*, 421–445.

(50) Scuseria, G. E.; Henderson, T. M.; Sorensen, D. C. The Ground State Correlation Energy of the Random Phase Approximation from a Ring Coupled Cluster Doubles Approach. *J. Chem. Phys.* **2008**, *129*, 231101.

(51) Eshuis, H.; Yarkony, J.; Furche, F. Fast Computation of Molecular Random Phase Approximation Correlation Energies using Resolution of the Identity and Imaginary Frequency Integration. *J. Chem. Phys.* **2010**, *132*, 234114.

(52) Macher, M.; Klimeš, J.; Franchini, C.; Kresse, G. The Random Phase Approximation Applied to Ice. *J. Chem. Phys.* **2014**, *140*, 084502.

(53) Del Ben, M.; VandeVondele, J.; Slater, B. Periodic MP2, RPA, and Boundary Condition Assessment of Hydrogen Ordering in Ice XV. *J. Phys. Chem. Lett.* **2014**, *5*, 4122–4128.

(54) Spreafico, C.; VandeVondele, J. The Nature of Excess Electrons in Anatase and Rutile from Hybrid DFT and RPA. *Phys. Chem. Chem. Phys.* **2014**, *16*, 26144–26152.

(55) Spreafico, C.; VandeVondele, J. Excess Electrons and Interstitial Li Atoms in TiO2 Anatase: Properties of the (101) Interface. *J. Phys. Chem. C* **2015**, *119*, 15009–15018.

(56) Del Ben, M.; Hutter, J.; VandeVondele, J. Probing the Structural and Dynamical Properties of Liquid Water with Models Including Non-Local Electron Correlation. *J. Chem. Phys.* **2015**, *143*, 054506.

(57) Cheng, J.; VandeVondele, J. Calculation of Electrochemical Energy Levels in Water using the Random Phase Approximation and a Double Hybrid Functional. *Phys. Rev. Lett.* **2016**, *116*, 086402.

(58) Olsen, T.; Yan, J.; Mortensen, J. J.; Thygesen, K. S. Dispersive and Covalent Interactions between Graphene and Metal Surfaces from the Random Phase Approximation. *Phys. Rev. Lett.* **2011**, *107*, 156401.

(59) Kim, M.-C.; Sim, E.; Burke, K. Understanding and Reducing Errors in Density Functional Calculations. *Phys. Rev. Lett.* **2013**, *111*, 073003.

(60) Voora, V. K.; Balasubramani, S. G.; Furche, F. Variational Generalized Kohn-Sham Approach Combining The Random Phase Approximation and Green¡80¿¡99¿s Function Methods. *Phys. Rev. A* **2012**, accepted.

(61) Ren, X.; Tkatchenko, A.; Rinke, P.; Scheffler, M. Beyond the Random-Phase Approximation for the Electron Correlation Energy: The Importance of Single Excitations. *Phys. Rev. Lett.* **2011**, *106*, 153003.

(62) Klimeš, J.; Kaltak, M.; Maggio, E.; Kresse, G. Singles Correlation Energy Contributions in Solids. *J. Chem. Phys.* **2015**, *143*, 102816.

(63) Al-Hamdani, Y. S.; Rossi, M.; Alfè, D.; Tsatsoulis, T.; Ramberger, B.; Brandenburg, J. G.; Zen, A.; Kresse, G.; Grüneis, A.; Tkatchenko, A.; Michaelides, A. Properties of the Water to Boron Nitride Interaction: From Zero to Two Dimensions with Benchmark Accuracy. *J. Chem. Phys.* **2017**, *147*, 044710.

(64) Erba, A.; Casassa, S.; Maschio, L.; Pisani, C. DFT and Local-MP2 Periodic Study of the Structure and Stability of Two Proton-Ordered Polymorphs of Ice. *J. Phys. Chem. B* **2009**, *113*, 2347–2354.

(65) He, X.; Sode, O.; Xantheas, S. S.; Hirata, S. Second-Order Many-Body Perturbation Study of Ice Ih. *J. Chem. Phys.* **2012**, *137*, 204505.

(66) Khaliullin, R. Z.; Cobar, E. A.; Lochan, R. C.; Bell, A. T.; Head-Gordon, M. Unravelling the Origin of Intermolecular Interactions using Absolutely Localized Molecular Orbitals. *J. Phys. Chem. A* **2007**, *111*, 8753–8765.

(67) Horn, P. R.; Mao, Y.; Head-Gordon, M. Probing Non-Covalent Interactions with a Second Generation Energy Decomposition Analysis using Absolutely Localized Molecular Orbitals. *Phys. Chem. Chem. Phys.* **2016**, *18*, 23067–23079.

(68) Zhu, Y.; Murali, S.; Cai, W.; Li, X.; Suk, J. W.; Potts, J. R.; Ruoff, R. S. Graphene and Graphene Oxide: Synthesis, Properties, and Applications. *Adv. Mater.* **2010**, *22*, 3906–3924.

(69) Lide, D. R. *CRC Handbook of Chemistry and Physics*; CRC Boca Raton, 2012.

(70) Becke, A. D. Density-Functional Exchange-Energy Approximation with Correct Asymptotic Behavior. *Phys. Rev. A* **1988**, *38*, 3098–3100.

(71) Lee, C. Development of the Colle-Salvetti Correlation-Energy Formual into a Functional of the Electron DEnsity. *Phys. Rev. B* **1988**, *37*, 785–789.

(72) Perdew, J. P.; Burke, K.; Ernzerhof, M. Generalized Gradient Approximation Made Simple. *Phys. Rev. Lett.* **1996**, *77*, 3865–3868.

(73) Perdew, J. P.; Ruzsinszky, A.; Csonka, G. I.; Vydrov, O. A.; Scuseria, G. E.; Constantin, L. A.; Zhou, X.; Burke, K. Restoring the Density-Gradient Expansion for Exchange in Solids and Surfaces. *Phys. Rev. Lett.* **2008**, *100*, 136406.

(74) Sabatini, R.; Gorni, T.; de Gironcoli, S. Nonlocal van der Waals Density Functional made Simple and Efficient. *Phys. Rev. B* **2013**, *87*, 041108.

(75) Sun, J.; Ruzsinszky, A.; Perdew, J. P. Strongly Constrained and Appropriately Normed Semilocal Density Functional. *Phys. Rev. Lett.* **2015**, *115*, 036402.

(76) Mardirossian, N.; Ruiz Pestana, L.; Womack, J. C.; Skylaris, C.-K.; Head-Gordon, T.; Head-Gordon, M. Use of the rVV10 Nonlocal Correlation Functional in the B97M-V Density Functional: Defining B97M-rV and Related Functionals. *J. Phys. Chem. Lett.* **2016**, *8*, 35–40.

(77) Becke, A. Density-Functional Thermochemistry. III. The Role of Exact Exchange. *J. Chem. Phys.* **1993**, *98*, 5648–5652.

(78) Betzinger, M.; Friedrich, C.; Blügel, S. Hybrid Functionals within the All-Electron FLAPW Method: Implementation and Applications of PBE0. *Phys. Rev. B* **2010**, *81*, 195117.

(79) Zhang, Y.; Yang, W. Comment on Generalized Gradient Approximation made Simple. *Phys. Rev. Lett.* **1998**, *80*, 890.

37

(80) Mardirossian, N.; Head-Gordon, M. ω B97M-V: A Combinatorially Optimized, Range-Separated Hybrid, meta-GGA Density Functional with VV10 Nonlocal Correlation. *J. Chem. Phys.* **2016**, *144*, 214110.

(81) Chai, J.-D.; Head-Gordon, M. Long-range Corrected Double-Hybrid Density Functionals. *J. Chem. Phys.* **2009**, *131*, 174105.

(82) Kristyán, S.; Pulay, P. Can (Semi) Local Density Functional Theory Account for the London Dispersion Forces? *Chem. Phys. Lett.* **1994**, *229*, 175–180.

(83) Hobza, P.; šponer, J.; Reschel, T. Density Functional Theory and Molecular Clusters. *J. Comput. Chem.* **1995**, *16*, 1315–1325.

(84) Grimme, S.; Ehrlich, S.; Goerigk, L. Effect of the Damping Function in Dispersion Corrected Density Functional Theory. *J. Comput. Chem.* **2011**, *32*, 1456–1465.

(85) Peng, H.; Yang, Z.-H.; Sun, J.; Perdew, J. P. SCAN+rVV10: A Promising van der Waals Density Functional. *Phys. Rev. X* **2016**, *6*, 041005.

(86) Boys, S. F.; Bernardi, F. d. The Calculation of Small Molecular Interactions by the Differences of Separate Total Energies. Some Procedures with Reduced Errors. *Mol. Phys.* **1970**, *19*, 553–566.

(87) Shao, Y.; Gan, Z.; Epifanovsky, E.; Gilbert, A. T. B.; Wormit, M.; Kussmann, J.; Lange, A. W.; Behn, A.; Deng, J.; Feng, X.; Ghosh, D.; Goldey, M.; Horn, P. R.; Jacobson, L. D.; Kaliman, I.; Khaliullin, R. Z.; Kús, T.; Landau, A.; Liu, J.; Proynov, E. I.; Rhee, Y. M.; Richard, R. M.; Rohrdanz, M. A.; Steele, R. P.; Sundstrom, E. J.; Woodcock III, H. L.; Zimmerman, P. M.; Zuev, D.; Albrecht, B.; Alguire, E.; Austin, B.; Beran, G. J. O.; Bernard, Y. A.; Berquist, E.; Brandhorst, K.; Bravaya, K. B.; Brown, S. T.; Casanova, D.; Chang, C.-M.; Chen, Y.; Chien, S. H.; Closser, K. D.; Crittenden, D. L.; Diedenhofen, M.; DiStasio Jr., R. A.; Dop, H.; Dutoi, A. D.;

Edgar, R. G.; Fatehi, S.; Fusti-Molnar, L.; Ghysels, A.; Golubeva-Zadorozhnaya, A.; Gomes, J.; Hanson-Heine, M. W. D.; Harbach, P. H. P.; Hauser, A. W.; Hohenstein, E. G.; Holden, Z. C.; Jagau, T.-C.; Ji, H.; Kaduk, B.; Khistyaev, K.; Kim, J.; Kim, J.; King, R. A.; Klunzinger, P.; Kosenkov, D.; Kowalczyk, T.; Krauter, C. M.; Lao, K. U.; Laurent, A.; Lawler, K. V.; Levchenko, S. V.; Lin, C. Y.; Liu, F.; Livshits, E.; Lochan, R. C.; Luenser, A.; Manohar, P.; Manzer, S. F.; Mao, S.-P.; Mardirossian, N.; Marenich, A. V.; Maurer, S. A.; Mayhall, N. J.; Oana, C. M.; Olivares-Amaya, R.; O'Neill, D. P.; Parkhill, J. A.; Perrine, T. M.; Peverati, R.; Pieniazek, P. A.; Prociuk, A.; Rehn, D. R.; Rosta, E.; Russ, N. J.; Sergueev, N.; Sharada, S. M.; Sharmaa, S.; Small, D. W.; Sodt, A.; Stein, T.; Stück, D.; Su, Y.-C.; Thom, A. J. W.; Tsuchimochi, T.; Vogt, L.; Vydrov, O.; Wang, T.; Watson, M. A.; Wenzel, J.; White, A.; Williams, C. F.; Vanovschi, V.; Yeganeh, S.; Yost, S. R.; You, Z.-Q.; Zhang, I. Y.; Zhang, X.; Zhou, Y.; Brooks, B. R.; Chan, G. K. L.; Chipman, D. M.; Cramer, C. J.; Goddard III, W. A.; Gordon, M. S.; Hehre, W. J.; Klamt, A.; Schaefer III, H. F.; Schmidt, M. W.; Sherrill, C. D.; Truhlar, D. G.; Warshel, A.; Xua, X.; Aspuru-Guzik, A.; Baer, R.; Bell, A. T.; Besley, N. A.; Chai, J.-D.; Dreuw, A.; Dunietz, B. D.; Furlani, T. R.; Gwaltney, S. R.; Hsu, C.-P.; Jung, Y.; Kong, J.; Lambrecht, D. S.; Liang, W.; Ochsenfeld, C.; Rassolov, V. A.; Slipchenko, L. V.; Subotnik, J. E.; Van Voorhis, T.; Herbert, J. M.; Krylov, A. I.; Gill, P. M. W.; Head-Gordon, M. Advances in Molecular Quantum Chemistry Contained in the Q-Chem 4 Program Package. *Mol. Phys.* **2015**, *113*, 184–215.

(88) Weigend, F.; Furche, F.; Ahlrichs, R. Gaussian Basis Sets of Quadruple Zeta Valence Quality for Atoms H–Kr. *J. Chem. Phys.* **2003**, *119*, 12753–12762.

(89) Frisch, M. J.; Pople, J. A.; Binkley, J. S. Self-Consistent Molecular Orbital Methods 25. Supplementary Functions for Gaussian Basis Sets. *J. Chem. Phys.* **1984**, *80*, 3265–3269.

(90) Rappoport, D.; Furche, F. Property-Optimized Gaussian Basis Sets for Molecular Response Calculations. *J. Chem. Phys.* **2010**, *133*, 134105.

(91) VandeVondele, J.; Krack, M.; Mohamed, F.; Parrinello, M.; Chassaing, T.; Hutter, J. Quickstep: Fast and Accurate Density Functional Calculations Using a Mixed Gaussian and Plane Waves Approach. *Comp. Phys. Commun.* **2005**, *167*, 103–128.

(92) Hutter, J.; Iannuzzi, M.; Schiffmann, F.; VandeVondele, J. CP2K: Atomistic Simulations of Condensed Matter Systems. *Wiley Interdiscip. Rev. Comput. Mol. Sci.* **2014**, *4*, 15–25.

(93) Goedecker, S.; Teter, M.; Hutter, J. Separable Dual-Space Gaussian Pseudopotentials. *Phys. Rev. B* **1996**, *54*, 1703–1710.

(94) Furche, F.; Ahlrichs, R.; Hättig, C.; Klopper, W.; Sierka, M.; Weigend, F. Turbomole. *Wiley Interdiscip. Rev. Comput. Mol. Sci.* **2014**, *4*, 91–100.

(95) Treutler, O.; Ahlrichs, R. Efficient Molecular Numerical Integration Schemes. *J. Chem. Phys.* **1995**, *102*, 346–354.

(96) Weigend, F.; Ahlrichs, R. Balanced Basis Sets of Split Valence, Triple Zeta Valence and Quadruple Zeta Valence Quality for H to Rn: Design and Assessment of Accuracy. *Phys. Chem. Chem. Phys.* **2005**, *7*, 3297–3305.

(97) Eshuis, H.; Furche, F. Basis Set Convergence of Molecular Correlation Energy Differences within the Random Phase Approximation. *J. Chem. Phys.* **2012**, *136*, 084105.

(98) Riplinger, C.; Sandhoefer, B.; Hansen, A.; Neese, F. Natural Triple Excitations in Local Coupled Cluster Calculations with Pair Natural Orbitals. *J. Chem. Phys.* **2013**, *139*, 134101.

(99) Neese, F. The ORCA program system. *Wiley Interdiscip. Rev. Comput. Mol. Sci.* **2012**, *2*, 73–78.

(100) Dunning, T. H. Gaussian Basis Sets for Use in Correlated Molecular Calculations. I. The Atoms Boron through Neon and Hydrogen. *J. Chem. Phys.* **1989**, *90*, 1007.

(101) Kendall, R. A.; Dunning Jr, T. H.; Harrison, R. J. Electron Affinities of the First-row Atoms Revisited. Systematic Basis Sets and Wave Functions. *J. Chem. Phys.* **1992**, *96*, 6796–6806.

(102) Halkier, A.; Helgaker, T.; Jørgensen, P.; Klopper, W.; Koch, H.; Olsen, J.; Wilson, A. K. Basis-set Convergence in Correlated Calculations on Ne, N2, and H2O. *Chem. Phys. Lett.* **1998**, *286*, 243–252.

(103) Helgaker, T.; Klopper, W.; Koch, H.; Noga, J. Basis-set Convergence of Correlated Calculations on Water. *J. Chem. Phys.* **1997**, *106*, 9639–9646.

(104) Hill, J. G.; Peterson, K. A.; Knizia, G.; Werner, H.-J. Extrapolating MP2 and CCSD Explicitly Correlated Correlation Energies to the Complete Basis Set Limit with First and Second Row Correlation Consistent Basis Sets. *J. Chem. Phys.* **2009**, *131*, 194105.

(105) Góra, U.; Podeszwa, R.; Cencek, W.; Szalewicz, K. Interaction Energies of Large Clusters from Many-body Expansion. *J. Chem. Phys.* **2011**, *135*, 224102.

(106) Liakos, D. G.; Sparta, M.; Kesharwani, M. K.; Martin, J. M.; Neese, F. Exploring the Accuracy Limits of Local Pair Natural Orbital Coupled-Cluster Theory. *J. Chem. Theory Comput.* **2015**, *11*, 1525–1539.

(107) Ran, J.; Hobza, P. On the Nature of Bonding in Lone Pair··· π-electron Complexes: CCSD(T)/Complete Basis Set Limit Calculations. *J. Chem. Theory Comput.* **2009**, *5*, 1180–1185.

(108) Eshuis, H. The Electron Correlation Methods Based on the Random Phase Approximation. *Theor. Chem. Acc.* **2012**, *131*, 1084.

(109) Kocman, M.; Pykal, M.; Jurečka, P. Electric Quadrupole Moment of Graphene and its Effect on Intermolecular Interactions. *Phys. Chem. Chem. Phys.* **2014**, *16*, 3144–3152.

TOC Figure